In situ x-ray reflectivity studies on the formation of substrate-supported phospholipid bilayers and monolayers

S. T. Wang,[1] M. Fukuto,[2,*] and L. Yang[1,†]
[1]*National Synchrotron Light Source, Brookhaven National Laboratory, Upton, New York 11973, USA*
[2]*Condensed Matter Physics and Materials Science Department, Brookhaven National Laboratory, Upton, New York 11973, USA*
(Received 21 December 2007; published 11 March 2008)

We conducted time-dependent, *in situ* x-ray reflectivity measurements on the formation of substrate-supported lipid monolayers and bilayers at solid-liquid interfaces, buried under an aqueous buffer with various concentrations (5, 10, 20, 40, and 50 μg/ml) of lipid 1,2-dioleoyl-sn-glycero-3-phosphocholine (DOPC). The DOPC bilayer is formed on the hydrophilic surface of a bare Si substrate, while the DOPC monolayer is formed on a hydrophobic octadecylthricholorsilane (OTS) monolayer-coated Si substrate. The evolution of the reflectivity curves from the lipid bilayers is well described by lateral growth of bilayer islands, consistent with the rupture and fusion model for the adsorption of lipid vesicles to solid-liquid interfaces. By contrast, the formation of the lipid monolayer on OTS-coated Si occurs through a relatively fast coverage of the entire interfacial area, followed by an increase in the monolayer thickness. For both monolayers and bilayers, the rate of lipid layer growth increases with increasing lipid concentration in the buffer solution.

DOI: 10.1103/PhysRevE.77.031909 PACS number(s): 87.16.D−, 87.14.Cc, 61.05.cm, 68.08.−p

I. INTRODUCTION

Phospholipid bilayers and monolayers are great experimental and theoretical models for biological membranes. Lipid layers have also been used as mobile substrate to facilitate two-dimensional (2D) ordering of proteins at the biofunctional interfaces. For example, phospholipid monolayers at the air-water interface have been used to facilitate the formation of 2D protein arrays; these structures have been transferred onto solid supports and subsequently studied by electron microscopy [1–5]. Recently, substrate-supported phospholipid monolayers and bilayers (SPLs) in aqueous solution have been attracting a great deal of attention [6–10]. This is partly due to the numerous advantages that SPLs have over liquid-supported films. For example, SPLs at solid-liquid interfaces are mechanically stable and are directly relevant to device applications like biosensors [9,10]. Moreover, SPLs have the advantage of greater ease in sample handling and benefit from the availability of *in situ* characterization tools such as atomic force microscopy (AFM) [11–13].

The preparation of substrate-supported phospholipid bilayers (SPBs) by spontaneous fusion of unilamellar lipid vesicles (ULVs) on solid supports was pioneered by Tamm and McConnell [14]. Since then, SPB formation on different surfaces has been investigated by a variety of techniques, such as fluorescence microscopy [15], AFM [12,16], quartz crystal microbalance [16,17], surface plasmon resonance [18], and neutron reflectivity [19]. However, these methods alone cannot completely resolve structural details such as the positions of molecular subunits (e.g., hydrophilic head groups and hydrophobic tails) along the bilayer normal or positions of embedded molecules in mixed systems with lipids, proteins, and other molecular species. X-ray scattering techniques are well suited for elucidating these details. Recent studies of SPBs have demonstrated the potential of x-ray reflectivity to probe the molecular structure of model lipid membranes [20–24].

In this paper, we report a detailed *time-resolved*, *in situ* x-ray reflectivity study elucidating the formation of substrate-supported lipid monolayers and bilayers at solid-liquid interfaces, buried under aqueous buffer with different concentrations (5–50 μg/ml) of 1,2-dioleoyl-sn-glycero-3-phosphocholine (DOPC). The evolution of the reflectivity curves from the DOPC bilayers formed on the hydrophilic surfaces of bare Si substrates is well described by lateral growth of bilayer islands, consistent with the "rupture and fusion" model for the adsorption of lipid vesicles to solid-liquid interfaces. By contrast, the x-ray results from the DOPC monolayer on a hydrophobic octadecylthricholorsilane- (OTS-) coated Si substrate show that the monolayer formation occurs through a relatively fast coverage of the entire interfacial area, followed by an increase in the monolayer thickness. The mechanisms for the growth of lipid bilayers and monolayers at the hydrophilic and hydrophobic liquid-solid interfaces, respectively, will be discussed.

In the following section, the sample preparation procedures and experimental techniques are described. In Sec. III, the experimental results and discussion are presented. In Sec. IV, the main conclusions are summarized.

II. EXPERIMENTAL METHODS

The DOPC lipid was purchased from Avanti Polar Lipids (Alabaster, AL). The OTS was purchased from Gelest Inc. (Morrisville, PA). Silicon wafers (⟨100⟩ surface, P-doped, 0.6 mm thick) were purchased from Virginia Semiconductor (Fredericksburg, VA). All materials were used as delivered.

In order to produce hydrophilic surfaces, silicon substrates (8×9 mm^2) were boiled in a solution of 70% H_2SO_4

*Corresponding author: fukuto@bnl.gov
†Corresponding author: lyang@bnl.gov

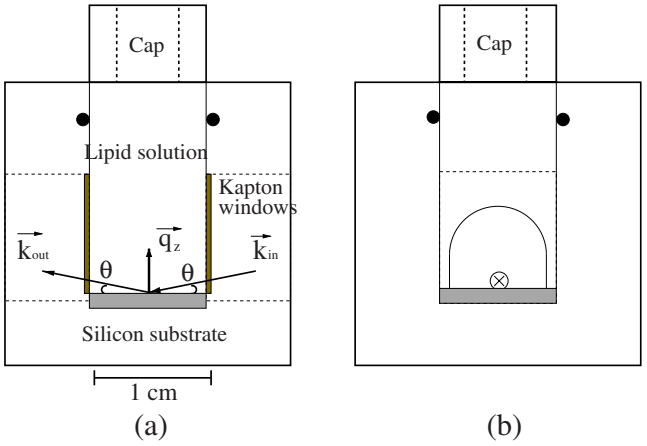

FIG. 1. (Color online) Schematic of the sample cell and the scattering geometry: (a) side view and (b) end-on view.

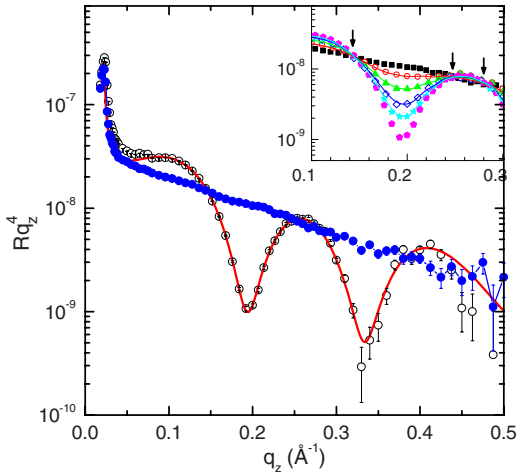

FIG. 2. (Color online) X-ray reflectivity data from a DOPC bilayer formed on a bare hydrophilic Si substrate ~16 h after injecting a 5-μg/ml DOPC lipid solution into the cell. The open circles are the data and the solid line is the best fit based on the three-slab model. The solid dots are the reflectivity data from a bare Si surface under the buffer solution. The inset shows reflectivity curves in a small q_z range (0.1–0.3 Å^{-1}) obtained at t=0 (black squares), 59 (red circles), 147 (green triangles), 264 (blue diamonds), 416 (cyan stars), and 936 min (purple pentagons) after injecting the lipid solution into the sample cell. The solid line for each transient data set in the inset is a superposition of the data sets for t=0 and 936 min. See text for details.

and 30% H_2O_2 for 20 min, rinsed thoroughly with Milli-Q water (18.2 MΩ cm), and stored in water prior to use. The hydrophobic, OTS-coated Si substrates were made by immersing the freshly cleaned hydrophilic Si substrates in a 5-mM bicyclohexyl solution of OTS and storing for ~18 h. The contact angle of water on OTS-coated substrates was typically >110°. The quality (thickness) of the self-assembled monolayer (SAM) of OTS on a Si surface was checked by x-ray reflectivity measurements prior to use.

Lipid solutions were made as follows. First, a lipid solution of known concentration in chloroform was dried in a vial by a nitrogen stream. The dried lipid was then kept in vacuum for 10 min to remove residual solvent and suspended in buffer solution by vortexing. The milky lipid suspension was then sonicated for about 30 min until it became transparent. During sonication, the vial containing the suspension was kept in an ice bath [12]. The buffer solution contained 2 mM $CaCl_2$, 150 mM NaCl, 10 mM HEPES, and 3 mM NaN_3, and the pH value was adjusted to 7.4 using NaOH solution [12]. The low-concentration lipid solution (5 μg/ml) was made by diluting the high-concentration solution (250 μg/ml) several times with buffer solution.

The *in situ* x-ray reflectivity measurements were performed at beamlines X22A and X6B of the National Synchrotron Light Source (NSLS). The scattering geometry and the sample cell are shown in Fig. 1(a). The Teflon sample cell was rinsed and sonicated in chloroform before the experiment. The x-ray energies were set at 32 keV (λ =0.385 Å) for X22A and 19 keV (λ=0.653 Å) for X6B, respectively. High-energy x rays were used in order to minimize x-ray absorption in water. As indicated in Fig. 1, x rays pass through a distance of about 1 cm in the solution. An 8 ×9 mm^2 Si substrate was fixed in the sample cell by a cap, where an o-ring was used to hold the cap in place and to prevent water leakage. The hole through the cap allows the lipid or buffer solution to be injected into the cell with a pipette or syringe. The total volume of liquid in the sample cell is about 0.8 ml. As shown in Fig. 1(a), in reflectivity measurements the outgoing angle is equal to the incident angle θ and the wave vector transfer along the surface normal q_z is given by $4\pi \sin\theta/\lambda$.

In order to ensure that time-dependent measurements be initiated with minimal time delay, the substrate was first aligned in air. The lipid solution was then added into the sample cell and the first reflectivity scan was started immediately, within 3–5 min. At the early stage of lipid layer formation, the reflectivity data were usually obtained every 15 min. After several hours, the data were taken every one hour. Between the scans, the x-ray beam was blocked to prevent the sample damage due to excessive x-ray exposure. It took about 20 min to obtain one complete reflectivity curve up to q_z=0.5 Å^{-1}. Since the structure changed faster at the beginning, the reflectivity measurements during the first several hours were mainly restricted to a smaller range of q_z (0.1–0.3 Å^{-1}), except that occasionally a complete reflectivity curve ($0.02 \leq q_z \leq 0.5$ Å^{-1}) was obtained for analysis purposes. All the measurements were carried out at room temperature (~25 °C).

III. RESULTS AND DISCUSSION

A. Bilayers on hydrophilic Si

Figure 2 shows, as open circles, the measured reflectivity curve from a complete DOPC bilayer, obtained 16 h after injecting a 5-μg/ml DOPC solution onto a hydrophilic Si/SiO_2 surface. For simplicity, we will hereafter use the term "Si" to imply the Si/SiO_2 surface with a native oxide layer. As a control, the reflectivity was also measured from a bare Si surface under the buffer solution before the formation of the bilayer, shown as the solid dots in Fig. 2. The appear-

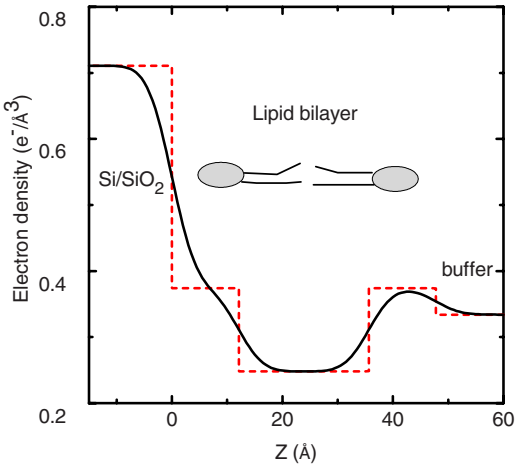

FIG. 3. (Color online) Average electron density profile (solid line) for a complete DOPC bilayer at the bare Si-buffer interface, corresponding to the best-fit reflectivity curve in Fig. 2. The dashed lines indicate the box model with three slabs between Si and the buffer.

ance of oscillations (Kiessig fringes) in the reflectivity after injecting the lipid solution clearly indicates the presence of a newly formed film on the Si surface. The inset of Fig. 2 shows reflectivity curves in a small q_z range obtained from intermediate stages at time $t=0$ (buffer solution), 59, 147, 264, 416, and 936 min after injecting the lipid solution. The inset clearly shows that the amplitude of Kiessig fringes increases with time and the dip at $q_z \simeq 0.2$ Å^{-1} becomes deeper until it reaches a minimum, consistent with growth of the lipid bilayer. One significant observation is that the q_z position of this dip remains fixed while the lipid bilayer grows. This implies that the thickness of the bilayer stays constant while either the average density in the bilayer or the surface coverage by the bilayer increases.

The solid line in Fig. 2 is the best fit to the final reflectivity data for the complete bilayer. The fit is based on the Parratt algorithm [25,26] and a three-slab model for the average electron density profile along the interface normal. The three slabs represent the head group of the inner lipid leaflet, the hydrocarbon tails of both leaflets, and the head group of the outer lipid leaflet. The electron density profile corresponding to the best fit is shown in Fig. 3. During the fitting, the electron densities of the water and silicon were fixed at $0.334e^-/$Å^3 and $0.711e^-/$Å^3, respectively. In order to reduce the number of fitting parameters, the two head group layers were constrained to have the same thicknesses and the same electron densities, and a single roughness parameter was used to describe the roughness of all the interfaces. The resulting best-fit parameters are listed in Table I. The electron density of the lipid tail, $\rho_t = 0.25e^-/$Å^3, is comparable to the published results, $(0.24-0.29)e^-/$Å^3, previously obtained for SPB by x-ray reflectivity [21,24] and for aligned multilayers by diffuse scattering [27]. The thickness of the hydrocarbon region, 23.5 Å, is in excellent agreement with 23.2 Å reported in Refs. [21] and the head-to-head distance of DOPC bilayer is found to be 35.6 Å, which is very close to the value of 37.1 Å obtained for DOPC multilayers [27].

TABLE I. Best-fit parameters for the reflectivity data for the complete DOPC bilayer in Fig. 2, based on a three-slab model and a four-slab model: layer thickness (d), electron density (ρ), and roughness (σ). The parameters for the water layer, the lipid head group, and the hydrocarbon tail layers are indicated by the subscripts w, h, and t, respectively. The data points for $q_z \geq 0.1$ Å^{-1} were included in the fits.

	Three-slab model ($\chi^2=4.1$)	Four-slab model ($\chi^2=2.1$)
d_w (Å)		4[a]
d_h (Å)	12.1 ± 0.4	6.1 ± 0.7
d_t (Å)	23.5 ± 0.8	27.5 ± 1.4
ρ_h ($e^-/$Å^3)	0.374 ± 0.005	0.45 ± 0.04
ρ_t ($e^-/$Å^3)	0.248 ± 0.005	0.244 ± 0.006
$\sigma_{\mathrm{Si/water}}$ (Å)		3.6[b]
σ (Å)	3.5 ± 0.1	5.0 ± 0.8

[a]Fixed, based on Refs. [21,22].
[b]Fixed, obtained from the best fit of Si/buffer reflectivity.

A four-slab model with an additional water layer between Si and bilayer was also used to fit the data. It produced a better fit than the three-slab model, but the improvement was not significant and the derived four-slab electron density profile was almost the same as the three-slab profile shown in Fig. 3. Moreover, when the thickness of the water layer was allowed to vary as a fitting parameter, the associated uncertainty exceeded the fitting value, signifying overparametrization. This implies that our data are not complete enough to justify the introduction of this additional water layer. However, as a reference, the best-fit parameters for the four-slab model with a 4-Å water layer [28] are also listed in Table I.

The fitting (not shown) of the reflectivity data acquired at different time during the bilayer formation confirms that the head-to-head distance of the bilayer remains constant to within ±0.5 Å at 35.6 Å, as expected. The analysis also demonstrates that as the bilayer grows, the average density of the head group sublayer increases whereas that of the hydrocarbon tail sublayer decreases. Because the electron density of water falls between the values for the hydrocarbon tail and the lipid head group, the observed evolution of the sublayer electron densities implies lateral growth of the lipid bilayer. On the basis of the electron density behavior alone, it would not be possible to distinguish between two possible bilayer growth mechanisms—namely, an increase in surface coverage by bilayer islands and an increase in local molecular packing density. However, the fact that the bilayer thickness remains fixed suggests that the growth is mediated by the formation and spreading of bilayer islands.

A key observation that provides further insights to the mechanism of bilayer formation is that all the reflectivity curves from the transient states share several common nodes, as indicated by the arrows in the inset of Fig. 2. This strongly suggests that all the reflectivity data may be described by linear superpositions of two reference reflectivity curves, with the nodes corresponding to the points where the two curves intersect. The obvious choices for the two reference points are the initial and final states of the bilayer

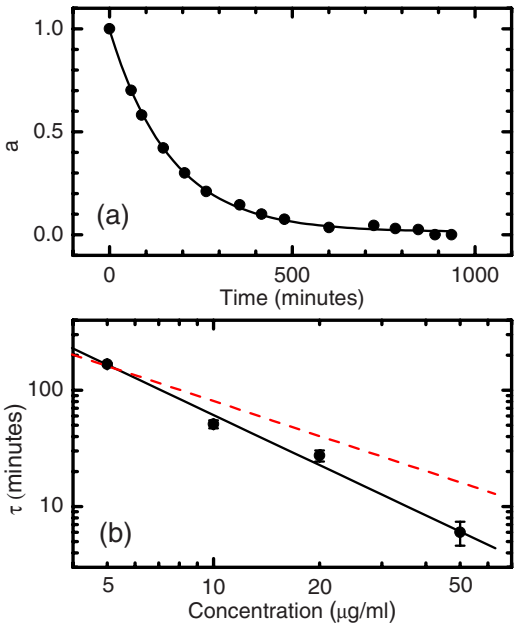

FIG. 4. (Color online) (a) The bare area fraction a as a function of time for bilayers formed under a 5-μg/ml DOPC lipid solution, based on the superposition method to reproduce the transient reflectivity data (see text for details). The solid line is a fit to exponential decay with the best-fit decay constant τ of 167.2 min. (b) τ as a function of the concentration of lipid solutions. The black solid line is the fit with a power-law form with the best-fit exponent of −1.4. The dashed line corresponds to a power law with an exponent of −1.

formation—namely, the reflectivity curve from the bare silicon-buffer interface (R_0) and the final reflectivity curve from a complete bilayer (R_1). We indeed find that all the reflectivity data from the transient states could be well reproduced by using the superposition $R=aR_0+(1-a)R_1$ and treating $0<a<1$ as the fitting parameter. For example, four superposition curves are shown as solid lines in the inset of Fig. 2. Physically, the parameter a ($a'=1-a$) is equal to the ratio of the bare, uncovered area (bilayer-coated area) to the total area on the Si surface. The uncovered area fraction a, obtained as a function of time for the 5-μg/ml DOPC lipid solution, is plotted as the dots in Fig. 4(a). The data can be fitted by an exponential decay function $e^{-t/\tau}$, shown as the solid line in Fig. 4(a). The decay constant τ is found to be 167.2 min for this particular lipid concentration.

We studied lipid solutions with various concentrations. For lipid solutions with high concentrations (>50 μg/ml), the bilayer formation process was too fast to be recorded by the reflectivity measurement, resulting in complete bilayer coverage within 10 min. The x-ray reflectivity curves of the final state are essentially independent of lipid concentrations, and they all exhibit the first minimum at $q_z \sim 0.20$ Å^{-1} within ± 0.01 Å^{-1}. The same analysis as described above for the 5-μg/ml solution was employed for the data from the 10-, 20-, and 50-μg/ml lipid solutions. The obtained decay constant τ as a function of lipid concentration is plotted in Fig. 4(b). The result clearly shows that the bilayer coverage occurs faster at higher lipid concentrations. As indicated by

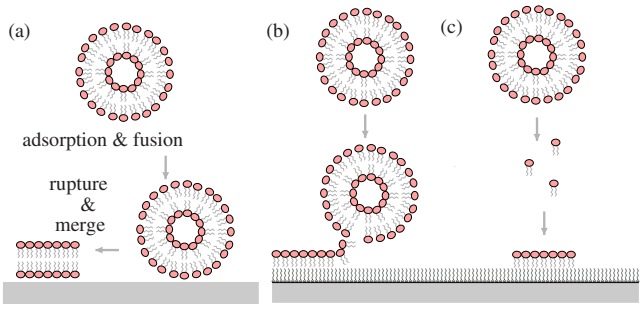

FIG. 5. (Color online) (a) An illustration of bilayer formation process through fusion and rupture of SUVs on a hydrophilic surface. (b) and (c) describe two possible processes: vesicle and monomeric adsorption for the formation of a monolayer on a hydrophobic OTS-coated surface.

the solid line in Fig. 4(b), the concentration dependence of the decay time approximately follows a power law with an exponent of -1.4 ± 0.1.

The bilayer formation process has been described well by the fusion and rupture model [15,16]. In this model, small ULVs adsorb to the surface first and then fuse to a large ULV, which then ruptures on the surface once its radius exceeds a critical radius R_c (50 nm$<R_c<$100 nm [16]). Large ULVs may directly adsorb onto the surface and rupture. The isolated bilayer patches will eventually merge together to form a complete bilayer on the surface. The process is illustrated in Fig. 5(a). Based on this picture, the exponential decay of uncovered area fraction a can be explained, at least qualitatively, by the following simple model. Denoting the concentration of the lipid solution (in mass/volume) by ρ and the lipid contribution to the average mass of a single unilamellar vesicle (SUV) by M_l, the average number of SUVs per volume is given by the ratio ρ/M_l. The typical lipid monomer concentration at critical micelle concentration (ρ_{cmc}) is on the order of 10^{-2} μg/ml [18,29], which is two orders magnitude lower than the lipid vesicle concentration in our system. For simplicity, we neglect the presence of lipid monomers and assume that all SUVs have the same size and they all drift with the same average speed $\bar{v}$ in the solution. If one SUV ruptures on the Si surface, the resulting bilayer island will cover a surface area S. The probability for a SUV to adsorb and rupture on the surface is denoted by P.

SUVs are drifting along all directions. Half of the vesicles move toward the substrate. On average, the component of the vesicle velocity ($\bar{v}$) toward the substrate is $\bar{v}/2$. In a given short time period dt, the uncovered surface area A changes by dA, which is equal to S times the number of vesicles that rupture on the surface: i.e.,

$$dA = -(1/2)SP(\rho/M_l)A(\bar{v}/2)dt. \quad (1)$$

Noting that a is equal to the ratio of the uncovered surface area A to the total area A_0 of the hydrophilic Si surface, integrating both sides of the above equation yields an exponential decay behavior for a:

$$a \sim A/A_o = e^{-PS\rho\bar{v}t/(4M_l)}, \quad (2)$$

$$\tau = 4M_l/(PS\rho\bar{v}). \quad (3)$$

The predicted inverse power-law dependence $\tau \propto \rho^{-1}$ of the decay constant on the lipid concentration, indicated by the dashed line in Fig. 4(b), is at least qualitatively consistent with the experimental result $\tau \propto \rho^{-1.4}$. The quantitative discrepancy between the derived and observed exponents is likely due to the simplicity of the model and the nonuniform size of SUVs.

Despite these shortcomings, the above simple model can be used to make a rough estimate of the adsorption probability P. Taking the typical lipid bilayer thickness to be $d=3.5$ nm and the SUV diameter to be about $D=200$ nm (twice as large as the reported R_c), the ruptured area of one bilayer island is $S=\pi(D-d)^2=1.21\times10^5$ nm^2. Taking the area per molecule to be 80 Å^2 in the bilayer, the mass of DOPC lipid bilayers in a SUV ($D=200$ nm) is $M_l=3.96\times10^{-16}$ g. For a $\rho=5$-μg/ml lipid solution, solving Eq. (3) for the average velocity of SUVs yields

$$\bar{v} = 4M_l/(PS\rho\tau) = 260.4/P(\text{nm/s}). \quad (4)$$

The average speed of a SUV can be estimated from the Brownian motion model. The mean-square displacement of a single Brownian particle [30] is

$$\langle(\Delta x)^2\rangle = 2k_BTt/(\pi\eta D). \quad (5)$$

Using $\eta=0.01$ poise for water, the average displacement of a vesicle ($D=200$ nm) over 1 s at room temperature is estimated to be $\sqrt{\langle(\Delta x)^2\rangle}\approx3600$ nm. Using Eq. (4), this translates into $P\sim0.07$ for the probability for a SUV to adsorb and rupture on the surface. It is likely that the low estimated value of P is partly due to the fact that P corresponds to the product of probabilities for both adsorption and rupture processes.

B. Monolayers on OTS-coated Si

Figure 6 shows the reflectivity data from OTS-coated Si (a) in air and (b) under buffer and from (c) a complete DOPC monolayer formed on the OTS film under a 5-μg/ml DOPC lipid solution. The reflectivity curve from the Si/OTS/air interface shows well-defined oscillations with a deep first minimum at $q_z=0.12$ Å^{-1}, indicating that the Si substrate is well covered by an OTS monolayer. Once the OTS-coated Si is immersed under buffer, the oscillation amplitude is reduced because the electron density contrast between buffer and the hydrocarbon chains is lower than that between air and the chains. After injecting the lipid solution, the first dip in the reflectivity curve shifts its position to lower q_z and becomes deeper, indicating the formation of an additional layer on top of the OTS monolayer.

In order to elucidate the structure of the DOPC monolayer, a four-slab model was used to fit the reflectivity data, with the four sublayers representing the OTS head group, the OTS tail, the lipid hydrocarbon tail, and the lipid head group. The best fit to the final reflectivity data from the lipid monolayer is shown as the solid line in Fig. 6(c). The thickness, electron density, and roughness of the OTS film were acquired by fitting the reflectivity curve from the Si/OTS/air interface using a two-slab model [31]. The best fit for this interface is shown as the solid line in Fig. 6(a), and its corresponding best-fit electron density profile is shown as the dashed line in Fig. 7. The data from the Si/OTS/buffer interface were fitted using a three-slab model [32], in which an additional depletion layer was added between the buffer and the OTS layer and the parameters for the OTS film were kept fixed at the best-fit values for the Si/OTS/air interface. The

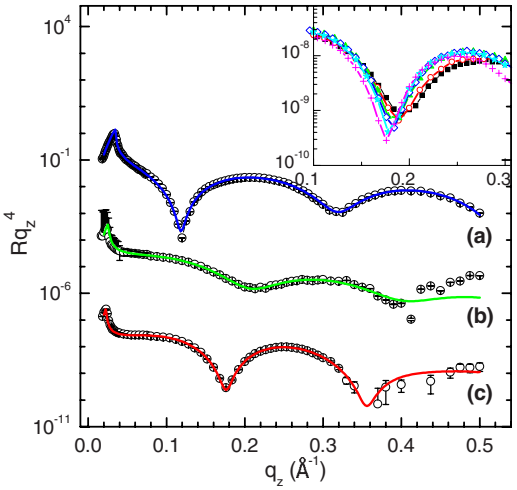

FIG. 6. (Color online) X-ray reflectivity data from (a) Si/OTS/air, (b) Si/OTS/buffer, and (c) Si/OTS/DOPC monolayer/buffer interfaces. The data in (c) correspond to a lipid monolayer formed on the hydrophobic OTS-coated Si approximately 11 h after injecting a 5-μg/ml DOPC lipid solution into the cell. The open circles are the data and the solid lines are the best fits. The curves are shifted vertically for clarity. The inset shows reflectivity curves in a small q_z range (0.1–0.3 Å^{-1}) obtained at $t=18$ (black squares), 51 (red circles), 111 (green triangles), 140 (blue diamonds), 189 (cyan stars), and 656 min (purple crosses) after injecting the lipid solution into the sample cell.

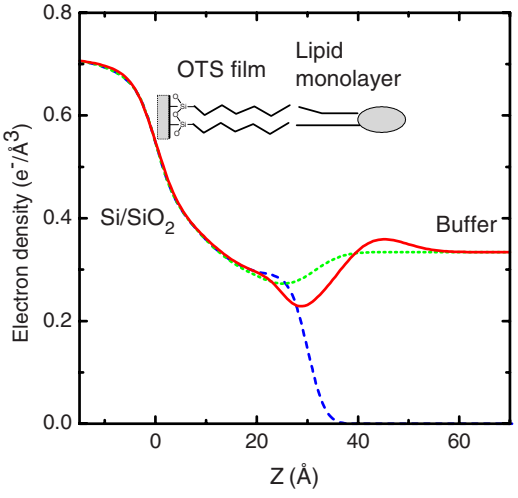

FIG. 7. (Color online) Average electron density profiles for Si/OTS/air (dashed line), Si/OTS/buffer (dotted line), and Si/OTS/DOPC monolayer/buffer (solid line) interfaces, extracted from the best fits to the reflectivity data shown in Fig. 6.

TABLE II. Best-fit parameters for the reflectivity data in Fig. 6: thickness (d), electron density (ρ), and roughness (σ). The subscripts 0–5 indicate layers corresponding to (0) the Si/SiO_2 substrate, (1) OTS head group, (2) OTS hydrocarbon tail, (3) lipid hydrocarbon tail, (4) lipid head group, and (5) the buffer, respectively. The data points for $q_z \geq 0.1$ Å^{-1} were included in the fits.

	Si/OTS/air ($\chi^2=7.1$)	Si/OTS/buffer ($\chi^2=5.4$)	Si/OTS/monolayer ($\chi^2=1.9$)
d_1 (Å)	4.0 ± 2.7	4.0[a]	4.0[a]
d_2 (Å)	26.1 ± 3.0	21.1 ± 8.0	21.3 ± 1.5
d_3 (Å)		5.3[b]	12.8 ± 3.2
d_4 (Å)			5.6 ± 3.3
ρ_1 (e^-/Å^3)	0.57 ± 0.09	0.57[a]	0.57[a]
ρ_2 (e^-/Å^3)	0.29 ± 0.02	0.29[a]	0.29[a]
ρ_3 (e^-/Å^3)		0.23[b]	0.20 ± 0.03
ρ_4 (e^-/Å^3)			0.49 ± 0.13
$\sigma_{0/1}$ (Å)	2.5 ± 1.4	2.5[a]	2.5[a]
$\sigma_{1/2}$ (Å)	9.0 ± 2.8	9.0[a]	9.0[a]
$\sigma_{2/3}$ (Å)	2.7 ± 0.5	5.5 ± 2.8	2.7[a]
$\sigma_{3/4,4/5}$ (Å)		4.6 ± 2.3	6.2 ± 3.5

[a]Fixed values are adopted from the best-fit parameters of OTS/air reflectivity.

[b]The error bars are larger than the fitting values. The fitting range 1.3–15.00 and 0–0.28 for d_3 and ρ_3, respectively, can give a reasonably good fitting.

best fit and the extracted electron density profile from the three-slab model are shown as the solid line in Fig. 6(b) and as the dotted line in Fig. 7, respectively. The obtained electron density and thickness values for the OTS monolayer listed in Table II are consistent with previously reported values [33–36]. By adding two slabs for the lipid monolayer (head and tails) on top of the Si/OTS/air profile and replacing the air with the buffer, a satisfactory fit is obtained for the reflectivity data from the lipid monolayer. The corresponding best-fit electron density profile for the complete lipid monolayer (the final state) is shown as the solid line in Fig. 7. The profile shows a dip in the electron density between the sublayers for the OTS tail and the lipid head group. This is likely due to the lower packing density of the DOPC tails relative to the all-*trans* tails for OTS and/or the lower electron density of the terminal methyl group relative to the methylene groups in the hydrocarbon tails [37].

The inset of Fig. 6 shows the evolution of the first intensity minimum in the reflectivity curves. As the monolayer grew, the depth of the dip increased until it reached the minimum. In addition, the q_z position of the dip ($q_{\min}$) shifted to lower q_z values before reaching a final constant value of 0.175 Å^{-1}. Since $q_{\min}^{-1}$ roughly scales with the thickness of the film on Si, the decrease in $q_{\min}$ reflects thickening of the monolayer. The time dependence of $q_{\min}$, shown in Fig. 8(a), can be described by an exponential decay behavior, but the associated decay time τ is much shorter than for the bilayer formation. The extracted decay constant of 55 min for the 5-μg/ml lipid solution is only one-third of the value obtained for the bilayer formation at the same lipid concentration. We also examined the effect of the lipid concentration on the rate of lipid monolayer thickening by tracking the reflectivity evolution under different lipid concentrations. Figure 8(b) shows the decay constants obtained for four different lipid concentrations. Unlike the case of the bilayer island formation on hydrophilic Si, the time constant for the thickening of the monolayer on the OTS-coated Si does not follow a power law, except possibly at low concentrations (<20 μg/ml), and appears to reach a constant value of $\tau \sim 10$ min at high concentrations.

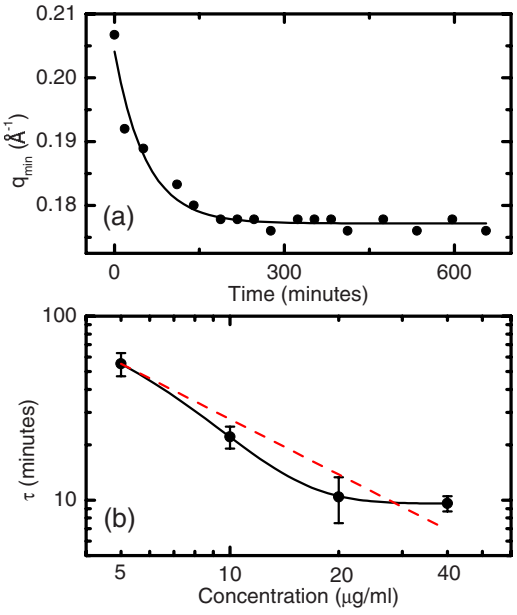

FIG. 8. (Color online) (a) Time dependence of the q_z position for the first minimum in the reflectivity curves from monolayers formed under a 5-μg/ml DOPC lipid solution. The solid line is a fit to exponential decay with the best-fit decay constant τ of 55 min. (b) τ as a function of the concentration of lipid solutions. The line connecting the dots is a guide to the eye. For reference, a power law with an exponent of -1 is drawn as the dashed line.

Extensive fitting has been carried out for all the reflectivity curves obtained from the lipid monolayer on OTS at different times. During the fitting, only the thickness and electron density of the two slabs for the lipid monolayer were allowed to vary. The fitting results qualitatively confirm that as the monolayer grows, the average thickness of the lipid monolayer increases and the densities of the two slabs vary monotonically toward the values for the final state.

Similar to the analysis for the bilayer formation, we also tried to use superposition of two reference reflectivity curves to reproduce all the transient reflectivity data. However, this approach did not produce acceptable fits, as expected from the absence of any common nodes in the plot of all the reflectivity curves. The use of the reflectivity curves for the Si/OTS/buffer interface and the complete lipid monolayer as the two reference states resulted in a large discrepancy between the superposition and the transient data. The superposition of another pair of two states—namely, the first reflectivity curve obtained immediately after the lipid injection and the final data from the complete monolayer—produced better fits, but a substantial discrepancy still existed between

the superposition and the data. Superposition of three states was also conducted, but the improvement was not significant.

The above observation demonstrates that the monolayer formation on the OTS-coated Si is very different from the bilayer formation on the hydrophilic Si. In particular, lateral growth based on island formation does not appear to apply to the monolayer formation. There are at least two possible processes that may be responsible for the lipid monolayer formation. First, lipid SUVs may diffuse to the hydrophobic surface and rupture to form a monolayer, as described in Fig. 5(b). Second, lipid monomers may diffuse to the surface and assemble the monolayer, as illustrated in Fig. 5(c). The first process is expected to be very slow because the adsorption of the vesicles (hydrophilic heads on the outside) onto the surface is inhibited due to the incompatibility between the hydrophilic periphery of the lipid vesicle and the hydrophobic OTS surface. Although the concentration of lipid monomers is low in solution ($\rho_{cmc} \sim 10^{-2}$ μg/ml) [29], the adsorption of monomers onto the hydrophobic surface is expected to be much faster than for vesicles. The experimental results presented above show that the formation of a lipid monolayer at the OTS/buffer interface occurs substantially faster than that of the bilayer on the hydrophilic Si. In addition, the apparent saturation of τ at high lipid concentrations ($\rho \geq 20$ μg/ml) is consistent, at least qualitatively, with the expectation that the *transient* or *local* concentration of monomers near the interface should be independent of ρ and close to the equilibrium value ρ_{cmc} ($\approx 10^{-2}$ μg/ml) as long as $\rho \gg \rho_{cmc}$. In view of these observations, it is likely that the monomeric adsorption is the dominant mechanism for the formation of the lipid monolayer. Furthermore, for the substrate size used, all the available lipid monomers at ρ_{cmc} are not sufficient to form a complete monolayer by themselves [38]. That is, the complete monolayer coverage of the substrate requires more lipid monomers to come from the dissociation from the vesicles. This dissociation process could be the rate-limiting step, and its time constant is on the order of minutes [18]. Therefore, τ includes not only the diffusion and adsorption of lipid monomers onto the surface, but also the dissociation of lipid monomers from the SUVs. On the basis of the above observations, we speculate that upon injection of the lipid solution onto the hydrophobic Si surface, a loosely packed monolayer immediately forms to cover the surface through monomeric adsorption. This is then followed by growth in both the thickness and packing density of the monolayer through one or both of the two processes above.

IV. SUMMARY

We have conducted real-time studies on the formation of a lipid bilayer on the hydrophilic Si-SiO_2 surface and a lipid monolayer on the hydrophobic OTS-coated Si surface using the x-ray reflectivity method. The formation process was monitored primarily through short scans over a small q_z range ($0.1-0.3$ Å^{-1}), together with occasional measurements over a wider q_z range ($0.02-0.5$ Å^{-1}). Detailed and time-dependent information on the growing process was obtained by fitting the reflectivity data at various times during the process. The evolution of the reflectivity curves from the lipid bilayers can be explained by an increased surface coverage through lateral growth of bilayer islands and is consistent with the rupture and fusion model for the adsorption of lipid vesicles to the solid/liquid interfaces. By contrast, the results suggest that the lipid monolayers form on OTS-coated Si through a relative fast coverage of loosely packed monomers on the entire interfacial area, followed by the thickening of the monolayer. The average electron density profiles for the complete lipid bilayers and monolayers that we obtained in the present study agree well with the results from previous studies [21,22,24,33–36].

ACKNOWLEDGMENTS

We thank our late colleague J. Baumert for his technical assistance and B. M. Ocko for his advice regarding the 32-keV measurements at NSLS Beamline X22A. The research was supported by a NSET grant from the DOE, No. DE-AC02-98CH10886. The experiments were carried out at the NSLS, BNL, which is supported by the DOE, Division of Material Sciences and Division of Chemical Sciences, under Contract No. DEAC02-98CH10886.

[1] P. Fromherz, Nature (London) **231**, 267 (1971).
[2] A. Brisson, A. Olofsson, P. Ringler, M. Schmutz, and S. Stoylova, Biol. Cell **80**, 221 (1994).
[3] O. D. Velev, Adv. Biophys. **34**, 139 (1997).
[4] S. A. Darst, M. Ahlers, P. H. Meller, E. W. Kubalek, R. Blankenburg, H. O. Ribi, H. Ringsdorf, and R. D. Kornberg, Biophys. J. **59**, 387 (1991).
[5] P. Ratanabanangkoon and A. P. Gast, Langmuir **19**, 1794 (2003).
[6] E. Sackmann, Science **271**, 43 (1996).
[7] J. T. Groves, N. Ulman, and S. G. Boxer, Science **275**, 651 (1997).
[8] A. F. Xie and S. Granick, Nat. Mater. **1**, 129 (2002).
[9] B. A. Cornell, V. L. B. Braach-Maksvytis, L. G. King, P. D. J. Osman, B. Raguse, L. Wieczorek, and R. J. Pace, Nature (London) **387**, 580 (1997).
[10] M. Tanaka and E. Sackmann, Nature (London) **437**, 656 (2005).
[11] S. Scheuring, D. J. Müller, P. Ringler, J. B. Heymann, and A. Engel, J. Microsc. **193**, 28 (1999).
[12] I. Reviakine and A. Brisson, Langmuir **16**, 1806 (2000).
[13] I. Reviakine and A. Brisson, Langmuir **17**, 8293 (2001).
[14] L. K. Tamm and H. M. McConnel, Biophys. J. **47**, 105 (1985).
[15] J. M. Johnson, T. Ha, S. Chu, and S. G. Boxer, Biophys. J. **83**, 3371 (2002).
[16] R.P. Richter and Alain Brisson, Langmuir **20**, 4609 (2004).
[17] C. A. Keller and B. Kasemo, Biophys. J. **75**, 1397 (1998).
[18] J. B. Hubbard, V. Silin, and A. L. Plant, Biophys. Chem. **75**,

163 (1998).
[19] T. Gutberlet, R. Steitz, G. Fragneto, and B. Klosgen, J. Phys.: Condens. Matter **16**, S2469 (2004).
[20] C. Reich, M. B. Hochrein, B. Krause, and B. Nickel, Rev. Sci. Instrum. **76**, 095103 (2005).
[21] C. E. Miller, J. Majewski, T. Gog, and T. L. Kuhl, Phys. Rev. Lett. **94**, 238104 (2005).
[22] E. Nováková, K. Giewekemeyer, and T. Salditt, Phys. Rev. E **74**, 051911 (2006).
[23] J. Daillant, E. Bellet-Amalric, A. Braslau, T. Charitat, G. Fragneto, F. Graner, S. Mora, F. Rieutord, and B. Stidder, Proc. Natl. Acad. Sci. U.S.A. **102**, 11639 (2005).
[24] M. B. Hochrein, C. Reich, B. Krause, J. O. Radler, and B. Nickel, Langmuir **22**, 538 (2006).
[25] L. G. Parratt, Phys. Rev. **95**, 359 (1954).
[26] J. Lekner, *Theory of Reflection* (Martin Nijhoff, Dordrecht, 1987).
[27] Y. Liu and J. F. Nagle, Phys. Rev. E **69**, 040901(R) (2004).
[28] The thickness of the water layer was reported as 4 Å in Refs. [21,22].
[29] D. Marsh, *CRC Handbook of Lipid Bilayers* (CRC Press, Boca Raton, 1990).
[30] P. M. Chaikin and T. C. Lubensky, *Principles of Condensed Matter Physics* (Cambridge University Press, Cambridge, England, 2000)
[31] For the OTS/air and OTS/buffer interfaces, one slab model did not produce acceptable fits, and the introduction of an additional slab was necessary to obtain reasonably good fits to the reflectivity data.
[32] We also tried a two-slab model to fit the data for the Si/OTS/buffer interface by (i) taking the best-fit profile for the Si/OTS/air interface, (ii) replacing the air with the buffer, and (iii) allowing the parameters for the OTS-tail slab to vary freely; however, this approach did not produce an acceptable fit to the data.
[33] I. M. Tidswell, B. M. Ocko, P. S. Pershan, S. R. Wasserman, G. M. Whitesides, and J. D. Axe, Phys. Rev. B **41**, 1111 (1990).
[34] I. M. Tidswell, T. A. Rabedeau, P. S. Pershan, S. D. Kosowsky, J. P. Folkers, and G. M. Whitesides, J. Chem. Phys. **95**, 2854 (1991).
[35] E. Frydman, H. Cohen, R. Maoz, and J. Sagiv, Langmuir **13**, 5089 (1997).
[36] S. Liu, R. Maoz, G. Schmid, and J. Sagiv, Nano Lett. **2**, 1055 (2002).
[37] B. M. Ocko (private communication).
[38] If all the available lipid monomers are adsorbed on the hydrophobic substrate surface, the area per lipid molecule is $A_0/(\rho_{cmc} \times 0.8 \times 6.02 \times 10^{23}/786.16) \sim 1000$ Å^2, where $A_0 = 72$ mm^2, $\rho_{cmc} \sim 10^{-2}$ μg/ml, the volume of sample cell is 0.8 ml, and the molecular weight of DOPC is 786.16 g/mol. This molecular area value is much larger than that for a complete DOPC bilayer (80 Å^2).